SUTCLIFFE, N. Slag/refractory and metal/refractory interactions during the production of stainless steels. *VII International Conference on Molten Slags Fluxes and Salts,* The South African Institute of Mining and Metallurgy, 2004.

Slag/refractory and metal/refractory interactions during the production of stainless steels

N. SUTCLIFFE
Columbus Stainless, South Africa

Refractories and slags play a vital role in the production of stainless steel. They are in intimate contact with the steel at temperature, and chemical reactions between the three can and do occur. These interactions can be beneficial, in the case of active tundish and ladle slags, and negative in the case of refractory erosion and slag entrapment. This paper presents the results of both plant trials and laboratory investigations of steel/refractory and slag/refractory interactions. The interaction mechanisms observed are described leading to selection criteria for new refractory products.

Keywords: slags, steels, refractories, reaction mechanisms.

Introduction

Columbus Stainless is situated in Middelburg, South Africa and is a subsidiary of Acerinox SA. The steel-making facilities currently consist of a 100-t EAF (with side tapping) two stationary 120-t bottom and top blown converters (one in use while the other is re-lined), ladle rinsing station and a straight mould, curved bow, continuous casting machine. The product range covers standard 300 and 400 grades as well as titanium-stabilized grades. The current throughput is 55 to 60 000-t per month, with 5% austenitic Ti-stabilized and 10% ferritic Ti-stabilized grades. More detail of the plant is given elsewhere[1–3].

The continual drive for increased throughput, improved quality and lower costs of production, necessitates the understanding of numerous variables. Two of these variables, namely refractory/slag and refractory/steel interactions, are the focus of this paper. Increased sequence length results in longer exposure of refractory to steel or slag, the effect being more erosion and chemical attack, which may influence quality. Higher quality refractory materials result in increased costs, thus a balance needs to be struck between costs, quality of the steel, and throughput.

Refractory properties play a vital role in their behaviour with slag and steel. These properties are both physical and chemical in nature, and extensive research has been conducted to understand the various mechanisms at play in the systems (refractory/steel and refractory/slag)[4–10]. The purpose of this work was to understand which mechanisms are at play within the system. The work also aimed to determine criteria for selection of new refractory products.

The main area of study in this work was the tundish, in terms of tundish working linings, tundish furniture and black refractories. The steel from the ladle enters the 25 T tundish via a refractory shroud with argon shielding between the collector nozzle and shroud. There is an impact pad and baffle in the tundish itself, and steel flow out of the tundish is controlled via a stopper rod system. Figure 1 shows the basic layout of the tundish and the position of the furniture. A detailed description of the tundish design and furniture set-up is given elsewhere[3].

Materials and experimental techniques

The first part of the work examined plant refractory samples from the tundish (used baffles, impact pads, black refractories and tundish linings). Samples were collected and studied under the SEM and the slag/refractory and steel/refractory interface reactions described. Subsurface tundish lining samples were studied to assess the level of slag coating that occurs during tundish draining[4–5]. This coating may then interact with the steel on the next heat and may be a source of inclusions in the steel.

The technique utilized for the laboratory work, was a simple dip test whereby samples of refractory were held in molten steel for pre-determined periods of time in an induction furnace. The samples were then prepared and analysed under the SEM (with EDS facility) to study the interface between the steel and refractory. This technique allowed a detailed description of the interactions to be made and also to determine the best refractory for the particular purpose to be selected.

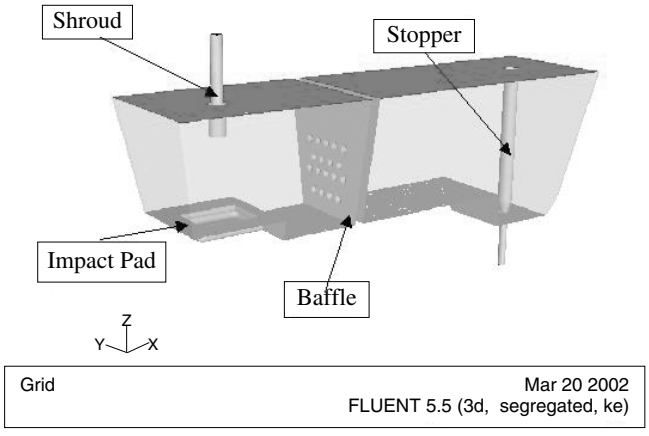

Figure 1. Basic tundish design and positions of furniture

Refractory bar samples, approximately 20 × 50 mm (cross-section) and 120 mm in length were suspended in a 20 kg induction furnace. The induction furnace was open to the atmosphere, and the crucible was MgO based. The samples were pre-heated for one hour at 1280°C and then transferred to the induction furnace. The 409 alloy, chemical analysis in Table I, was held at 1600°C. The high operating temperature was utilized to ensure a severe attack within the ten-minute period of submergence. The short test period was utilized to limit the decarburization of the refractories and thus maintain a stable C level in the steel. The chemistry of the melt was analysed after each test and corrected to ensure relatively stable experimental conditions. The effects of chemical changes, such as decarburization of the refractory, were not assessed in this work. After submergence, the samples were allowed to cool in air. The steel samples were ground on P80 grit Al_2O_3 paper and polished on P180 grit Al_2O_3 paper and analysed by means of the ARL9800 XRF technique. The carbon was analysed by means of a Leco CS400 optical emission spectrometer with a relative accuracy of 0.003 wt%. The oxygen and nitrogen were analysed by means of a Leco T316 OES, with a standard deviation of ±2 ppm.

Samples for SEM analysis were prepared to a 3 mm finish using standard metallographic techniques and coated with a thin layer of gold for conductivity

Slag samples taken from the plant (Table I) were milled to a 150 mm particle size, then briquetted, and the chemistry was analysed with an XRF fluorescence method (ARL9800 wavelength dispersive instrument) to determine the oxide compositions. The standard deviation for oxides in the slag ranges between 0.1 and 1 wt% dependent upon the particular oxide (CaO = 0.9%, Al_2O_3 = 0.3%, MgO = 0.1%, SiO_2 = 1%).

Wet chemical analysis of the un-reacted materials was performed via lithium tetraborate fusion–ICP/OES technique. Table II gives the chemical analysis of all refractories utilized in the current study. Table III shows the mechanical/physical properties of the refractories.

SEM/EDS analysis was conducted on all raw materials and samples prior to the plant and laboratory tests. The main phases present in the various products are shown in Table IV with Tables V and VI showing the post reaction phases observed.

Black refractories

Three distinct types of black refractory were tested in the laboratory:

- Al_2O_3-SiO_2-C refractories—D99, D90, D63 and V101
- MgO-C refractory—DM4
- ZrO_2-C—Z6 and Z62

Castables

The dip tests were utilized to study the MgO based castable products, Table II samples M1 and M2. The plant sample was an Al_2O_3-SiO_2 based product (L17), and was compared in the un-reacted and reacted states with M1 and M2. L17 is utilized in the manufacture of both the impact pad and baffle, a plant sample was taken and analysed after a 4-ladle sequence of 409 material.

Linings

Three types of tundish lining material were studied in the current work. The first, T1, was a standard spray material; the second an 'active' spray material applied on to the standard spray material (T2); and thirdly, a 'dry-vibe' material (T3). Samples were taken from the tundish slag line area and from the steel/refractory contact area.

Table I
409 alloy chemistries (wt. %) and plant slag analyses

Sample	C	S	Si	Mn	Cr	Ni	Co	Ti	N	O	Al	Mo	P
Lab	0.023	0.005	0.5	0.2	11.5	0.1	0.1	0.24	0.020	0.005	0.003	0.1	0.025
Plant	0.011	0.002	0.55	0.3	11.6	0.15	0.1	0.18	0.010	0.003	0.005	0.1	0.019

Sample	CaO	MgO	SiO_2	TiO_2	MnO	Cr_2O_3	Al_2O_3
Start	34.4	4.36	35.9	4.18	1.35	1.43	16.3
End	34.5	3.98	27.0	17.2	1.33	1.35	15.8

Table II
Chemical composition of refractory samples

Sample	Al_2O_3	TiO_2	SiO_2	CaO	MgO	ZrO_2	Total C	Other
D90	51.00	0.9	14.00	0.30	0.60	1.8	32.00	
D99	58.70	0.8	10.20	0.20	0.30	0.6	31.50	
DM4	2.20	-	6.30	1.60	69.0	0.3	16.00	
D63	61.50	0.8	10.00	0.20	0.3	4.5	24.50	
Z6	0.30	-	8.00	2.40	0.2	74.5	16.50	
Z62	0.30	-	7.00	2.00	0.2	75.0	14.50	
T2	0.82	0.01	4.35	21.60	65.3		0.935	Fe_2O_3 : 2, + Binder
T3				1.70	92.0	3.2		Fe_2O_3 : 2, + Binder
M1	0.22		10.50	2.08	88.4			Fe_2O_3 : 1
L17	64.00		33.00	0.60	0.6			Fe_2O_3 : 0.5
M2	0.60	0.2	5.90	2.60	90.7			
V101	52.00		15.70				31.20	Fe_2O_3 : 0.5, B_2O_5 : 1.6
T1	1.50	0.5	5.00	2.00	87.2			Bal: Metal Oxides

Table III
Mechanical properties of refractory samples

Sample	Rupture MN/m²	W/mK	Density g/cm³	Apparent porosity
D90		18	2.27	19.5
D99	9.0		2.43	18.0
D63		18	2.60	18.5
V101	7.4		2.35	17.9
DM4	5.4		2.50	18.0
Z6	6.5	13	3.55	16.3
Z62	10.0	13	3.66	12.6
T1	4.0	4	2.65	36.5
T2			1.75	
T3	4.0		1.85	
M1	6.0		2.70	25.0
M2	7.0		2.90	20.0
L17	10.2		3.00	

Table IV
Phases present in the refractory samples before reaction

Sample	Species present
D90	Al_2O_3 grains, graphite flakes, SiO_2 particles
D99	Al_2O_3 grains, graphite flakes, SiO_2 particles, finer grain size than D90 and D63
D63	Al_2O_3 grains, graphite flakes, SiO_2 particles, ZrO_2 grains
V101	Al_2O_3 grains, graphite flakes, SiO_2 particles, Si metal, grain size as per D99
DM4	MgO grains, graphite flakes and small particles of $Al_2O_3.SiO_2$
Z6	ZrO_2 , graphite flakes, small particles of SiO_2
Z62	ZrO_2 , graphite flakes, small particles of SiO_2
T1	MgO grains bound together by $CaO.MgO.SiO_2$ or $CaO.SiO_2$
T2	MgO grains with some $CaO.SiO_2.MgO$ bounds between particles. Small quantity of $Al_2O_3.SiO_2$
T3	MgO grains, matrixes of CaO, $CaO.SiO_2$ and $CaO.MgO.SiO_2$
M1	MgO grains in a $MgO.SiO_2.CaO$ matrix (Average MgO grain size: 500 µm)
M2	MgO grains in a $MgO.SiO_2.CaO$ matrix (Average MgO grain size: 100 µm
L17	$Al_2O_3.SiO_2$, $CaO.Al_2O_3$, Al_2O_3, Fe-Ti oxide phase

Table V
Phases found in steel/refractory reaction zones and not seen in the un-reacted state

Sample	Species present
D90	Al-Si-Ti-O, Fe-Si-Ti and Cr-Mn-Ti metal particles
D99	Ti rich Ti-Si-O, Ti-Si rich Ti-Si-Al-Mg-O, Fe-Cr metal particles
D63	Ti rich Ti-Al-O, Al rich Al-Si-O
V101	Metal particles, Ti rich Ti-Si-O
DM4	Mg rich Mg-Al-O-Ti, Mg rich Mg-Si-O, Cr and Ti metal particles
Z6	Al rich Al-Zr-O and Zr rich Al-Zr-O, Si-Ca-Ti-O, Zr-Ti-O, Si-Zr-Ca-O
Z62	Al rich Al-Zr-O and Zr rich Al-Zr-O, Si-Ca-Ti-O, Zr-Ti-O, Si-Zr-Ca-O
T1	Cr-Ti-Al-O, $CaO-TiO_2$
T2	$CaO-TiO_2$, Ca rich Ca-Si-Mg-O, steel particles,
T3	Cr rich Cr-Ti-Al-O, $CaO-TiO_2$
M1	Ti rich Ti-Si-Ca-O, Ti rich Ti-Mg-O
M2	Ca rich Ca-Ti-Si-Mg-O, Mg-Ti-O,
L17	Al-Si-Ca-O, Al rich Al-Si-Mg-Cr-Mn-O, $CaO-TiO_2$ particles

Table VI
Phases found in slag/refractory area and not seen in the un-reacted state

Sample	Species present
V101	$CaO.TiO_2$
T1	$CaO.TiO_2$,
T3	Ca rich Ca-Si-O, Cr-O

Table VII
Steel and slag penetration depths

Sample	Steel penetration mm	Slag penetration mm
D90	2.50	-
D99	0.50	-
D63	2.00	-
V101	0.50	0.20
DM4	2.00	-
Z6	3.00	-
Z62	2.00	-
T1	3.00	2.0
T2	3.50	-
T3	0.15	3.50
M1	3.50	-
M2	4.00	-
L17	1.25	

Results and discussion

Black refractories

The Al_2O_3-SiO_2-C refractories have a range of 51 to 61% Al_2O_3, 10 to 16% SiO_2, and 24 to 3% C. The depth of penetration of the refractory by the steel is shown in Table VII. The direct affect of C content is not determinable from these tests, but can be inferred from the reaction products seen on the samples. Cirilli *et al*[10] and Kwon *et al.*[11] discussed the reduction of refractory oxides by carbon in the refractory, leading to changes in the rate of C dissolution when a refractory is in contact with a steel at temperature. The final effect of the C dissolution is to produce oxides in the steel, which are then deposited on the refractory. The proposed reactions are shown in Equations [1] to [5]. (The phase conventions used in the following reactions are: <x> refractory/slag component 'x'; [i] component 'i' in the steel; {y} gaseous component 'y'.)

$$3 < SiO_2 > +3 < C > +4[A1] = 2 < Al_2O_3 > +3[Si] + 3[C] \quad [1]$$

$$5 < SiO_2 > +5 < C > +3[Ti] = \ < Ti_3O_5 > +5[Si] + 5\{CO\} \quad [2]$$

$$< SiO_2 > + < C > \ = \{SiO\} + \{CO\} \quad [3]$$

$$< MgO > + < C > \ = \{Mg\} + \{CO\} \quad [4]$$

$$< ZrO_2 > +3 < C > = \ < ZrC > +2\{CO\} \quad [5]$$

$$< Al_2O_3 > +[Mg] + [O] = \ < MgO.Al_2O_3 > \quad [6]$$

The products of reactions [1] and [2] were seen on the samples in the current work as well as in the spinel as presented in reaction [6]. To achieve the products seen in this work, reactions [3], [4] and [5] are the steps required. The complex nature of the network, and presence of Si, Cr, Mg etc, complicates the mechanism, and can be assumed to be the effect of solid solution substitution.

The work of Kwon *et al.*[11] investigated the effect of Ti and Al contents of ultra low carbon steels on Al_2O_3-SiO_2-C refractories. In the work, they found Al and Ti oxide based networks on the refractory, due to decarburization of the refractory and subsequent oxidation of Al and Ti in the steel. Lehmann *et al.*[12] investigated the interaction of Al and Ti containing ultra low carbon steels on MgO-C refractories. Here they found similar reduction reactions and dense layer formation, in this case $MgO.Al_2O_3$ spinel. In the current work, Ti and Al are associated with complex structures (Table V), with V101 showing only Ti in a Ti-Si-O phase. The quantities of Ti and Al in the complex phases vary, hence Table V states which element is the most dominant. In the current work the carbon gradient from refractory to steel was lower, the emersion time shorter and the SiO_2 content of the refractory was significantly lower than that in the work of Kwon *et al.*[11] thus the differences in network formation.

The morphology and distribution of phases, as well as the physical properties of D90, D99, D63 and V101, affect the steel penetration depth to varying degrees, Table VII. The main difference between D90 and D99 is the size of the Al_2O_3 grains, with D90 showing grain sizes up to 1 mm versus 0.5 mm for D99. V101 has grains < 0.4 mm with a finer, overall distribution, when compared to D99. Figure 2 shows the D99 sample, with a higher magnification photomicrograph showing various reaction products in the penetration zone. The D90, D63 and V101 samples also show similar structures and phases; the penetration depth is the key difference as outlined in Table VII. All 4 samples show metal particles of Fe-Cr and Cr-Mn-Ti.

Both D63 and D90 have small quantities of ZrO_2, but as explained below, the destabilization of ZrO_2 affects the penetration greatly by producing finer grains with larger network areas allowing easier penetration. Matsushita *et al.*[13] proposed a modification to the capillary model[7] for penetration in a porous refractory. The modification utilizes a 'labyrinth' factor to produce a prediction closer to the experimental values. It may be extrapolated to the current work to cover the penetration of the refractory between the grains; the larger the grains the smaller the network paths and, with continual reaction with time, the ZrO_2 will destabilize and produce a larger network and increase the penetration.

Figure 3 shows the slag/refractory reaction zone for V101. The slag shows minimal penetration, with no evidence of reaction between the slag and the Al_2O_3 grain. The particular plant sample under investigation was from the shroud, and the metallic blebs, entrapped in the slag, show the influence of turbulence in the shroud area. There is no evidence of densification of the refractory due to exposure to temperature over a one-hour period. The current SEN (submerged entry nozzle) is made from V101, and after 14 hours the inner lining shows minimal erosion, and samples have indicated only a small interaction zone (<0.5 mm).

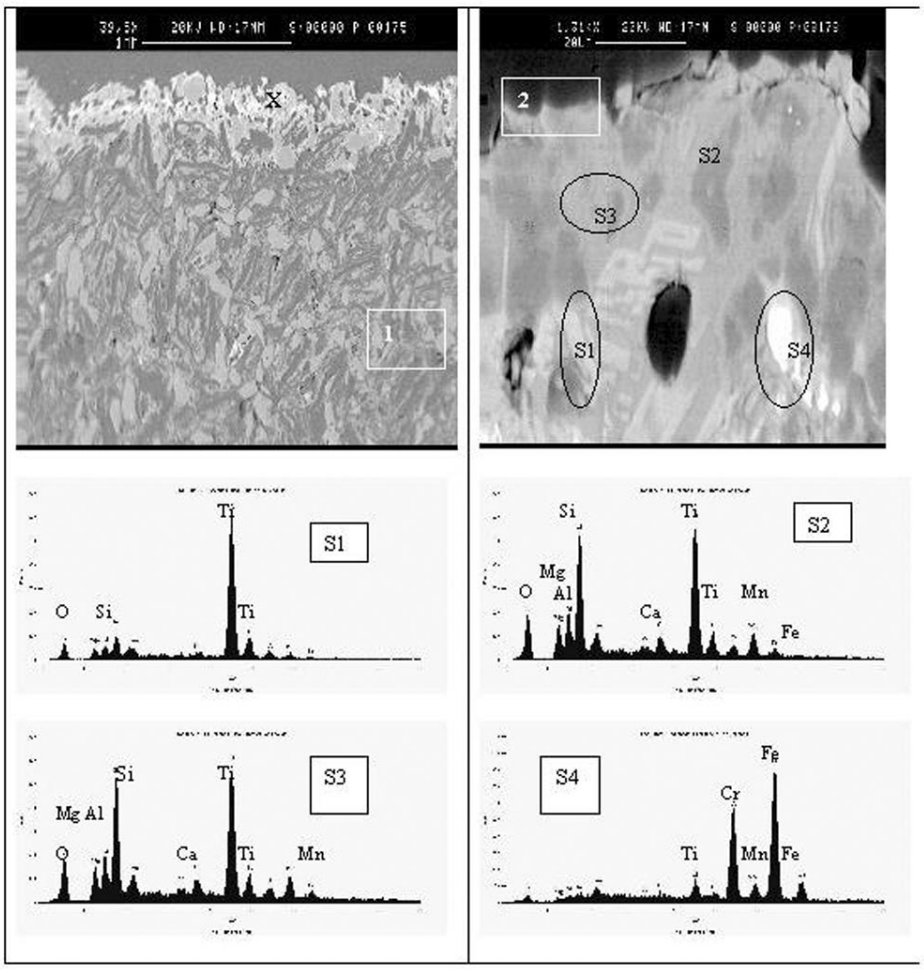

Figure 2. Sample D99. Micrograph 1 is at low magnification, and micrograph 2 is a higher magnification of X. S1, S2 and S3 show various Ti-O-X phases (X = Mg, Al, Cr, Mn, Ca) within the matrix. S4 shows an entrapped Fe-Cr metallic bleb

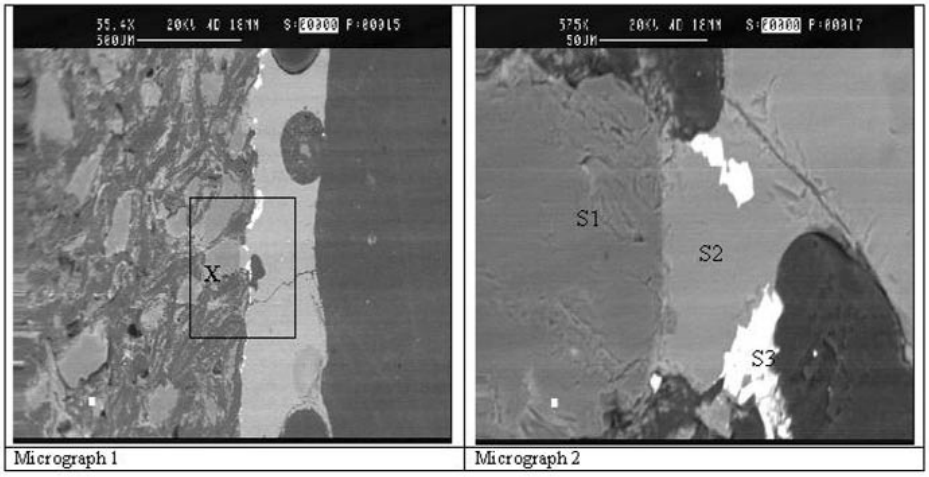

Figure 3. V101 Slag/refractory interface sample. Micrograph 1 shows a low magnification of the surface and 2 is a higher magnification micrograph of position X in 1. S1 is an Al_2O_3 grain, S2 is $CaO.SiO_2$ from the slag and S3 is a metallic bleb

Recently, there have been developments of Doloma based refractories for submerged entry nozzles (SEN) with the rationalization being the reduction of alumina clogging[14–15]. To the author's knowledge there has not been a published report on the utilization of MgO based SENs in the production of stainless steel. The lack of tube changing facilities at Columbus thus raises the risk of aborted casting if any unexpected problems arise during a plant trial. The laboratory dip tests gave an indication of how an MgO based refractory may behave in a 409 steel. Nunnington and Sutcliffe[2] described the clogging mechanism associated with the production of 409 steel at Columbus. They outlined that there was almost invariably a reaction interface with the alumina-graphite refractory of the SEN. Detailed SEM examination of the carbon depleted interface showed the formation of oxy-nitrides and Al_2TiO_5, indicating that the initial reaction involved TiN reacting with SiO_2 in the zirconia-mullite phase in the refractory matrix. It was also found that the 3-dimensional network in a 409 clog had a bonding phase of $MgO.Al_2O_3$ spinel with the matrix. The extremely fine (sub-micron) size and distribution of the spinel indicated it had formed in the steel as it passed through the SEN, rather than already being present as an inclusion. In effect, the spinel formed a sub-network within the clog. A proposed reaction for this spinel is shown in Equation [6].

Several authors[8,10,12] have proposed that MgO is reduced by C in the refractory, thus aiding Reaction [6]. Figure 4 shows the interaction layer formed and the associated EDS analyses of DM4. Three distinct phases are present: MgO (periclase grain), an Mg-Si-O phase and an Mg-Ti-Al-O phase. It is proposed that the short test duration and rapid cooling of the test piece (relative to a SEN in the plant environment) was insufficient for a distinct $MgO.Al_2O_3$ spinel to form. The oxide phases formed will lead to localized under-cooling, allowing freezing of the steel and the associated build up of clogging material[2]. The presence of Cr, Si and Ti in the refractory sample to a depth of over 2 mm, is concerning when compared to an MgO tundish lining material (T1) which showed a maximum steel penetration of 3 mm after 4 hours' exposure to a 409 steel in the plant.

The MgO grains in the un-reacted doloma based refractory had a size distribution of 50 μm up to 2 mm. Post reaction, the grain size distribution in the penetration zone had decreased to a 10 μm to 1 mm range, thus indicating a potential reduction of MgO by the graphite in the refractory. Significant porosity can also be seen in Figure 4, highlighting the severe attack of the refractory. With high steel velocities through the SEN, erosion of this porous layer could result in increased inclusion loading as well as thinning of the refractory wall. The porous layer will also change the heat transfer through the SEN and affect steel deposition and thus further reactions with the refractory.

The zirconia based refractories (Z6 and Z62) displayed similar chemical analyses, with similar penetration results, Table VII. Z62 has a higher density and lower apparent porosity than Z6 due to the distribution of the graphite flakes, Figure 5. The interface zone on both samples show a Si-Ca-Ti-O phase between the zirconia grains. There is more porosity in the reaction zone of Z62, however, the penetration extent is slightly less than Z6. The porosity is of concern, as the removed particles will enter the steel, thus increasing the inclusion loading. Vermeulen *et al*.[15] did not find porosity in samples of ZrO_2 in contact with steel. The presence of the porosity in this test work is potentially attributable to one of three mechanisms or a combination of the three:

- The dissolution of carbon from the refractory allows penetration of the matrix by steel, leading to the ZrO_2 particles being washed out
- The reaction of Ti in the alloy with SiO_2 in the refractory, leading to steel penetration along the matrix paths between the ZrO_2 particles
- Destabilization of zirconia due to changes in the activities of oxides in the matrix surrounding the zirconia grains.

In the work of Nunnington and Sutcliffe[2] the reduction of SiO_2 by Ti at the steel/slag interface, as well as reduction of SiO_2 from refractories, is described in detail. In the current case, the presence of the Si-Ca-Ti-O phase in the matrix surrounding the ZrO_2 grains supports the second mechanism for porosity. Lee and Sunwoo[16] tested calcium, magnesium and yitria stabilized zirconia graphite, in contact with synthetic mould powders. The affect of SiO_2 and CaO on the zirconia is to cause destabilization leading to the formation of a monoclinic zirconia phase. In dip tests in steel, Lee and Sunwoo[16] found that the presence of SiO_2 decreases the activity of CaO in the matrix, producing a

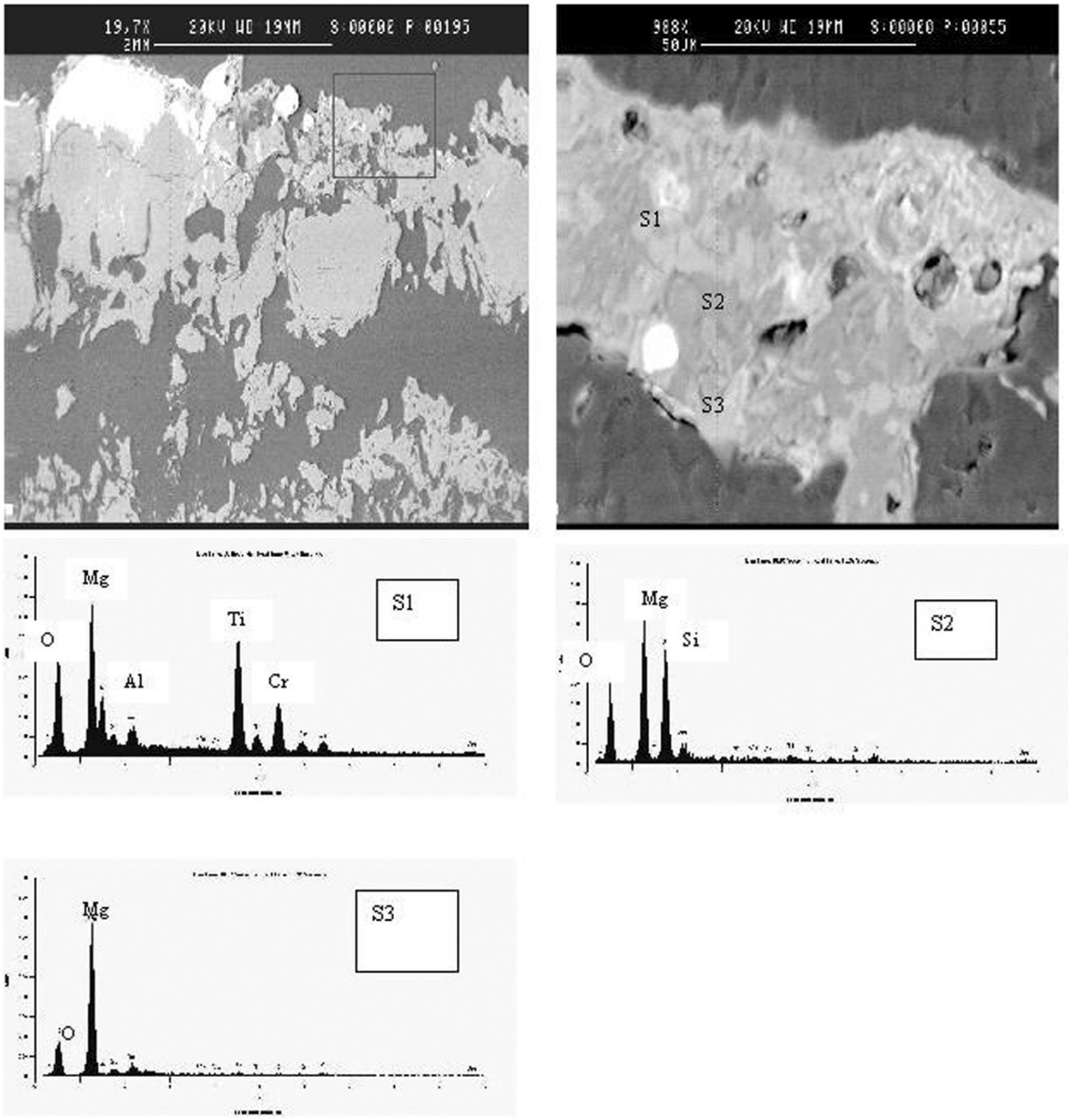

Figure 4. Photomicrographs showing a low magnification of the reacted MgO-C black refractory (DM4) as well as a high magnification and the associated EDS analyses

CaO chemical potential gradient in the stabilized zirconia particle. The presence of TiO_2 in this work, formed from the reduction of SiO_2, will decrease the CaO activity further, thus increasing the deterioration of the zirconia refractory.

The initial ZrO_2 grain sizes for both Z6 and Z62 were in the range of 50 µm to 1.5 mm. In the penetration zone, the grain size decreases to a 10 µm to 1 mm range, with a higher proportion of the grains in the 10 to 100 µm range. Based on the work of Lee and Sunwoo[16], the destabilization of zirconia appears to have occurred in these tests. Uchida[17] studied the effect of ZrO_2 grain size on the corrosion resistance of zirconia graphite refractories. Uchida[17] found that a coarse grain structure, with low bulk density and high apparent porosity, results in high erosion, even with a high ZrO_2 content.

The grain size and distribution of ZrO_2 as well as the presence of SiO_2 in the mix will affect the penetration and erosion of the refractory. Extrapolating to the protection band of SENs in contact with mould powder indicates that careful consideration of the structure of the refractory must be taken into account rather than purely the chemical analysis.

Castables

Traditionally, tundish furniture, baffles, dams, weirs and impact pads have been produced from Al_2O_3 based castable refractories. The current tundish furniture at Columbus utilizes the L17 material shown in Table II. Samples of MgO based castables were received from two suppliers and utilized in the dip tests. Severe macro damage/erosion was noted on M1 after the dip test and was as a result of

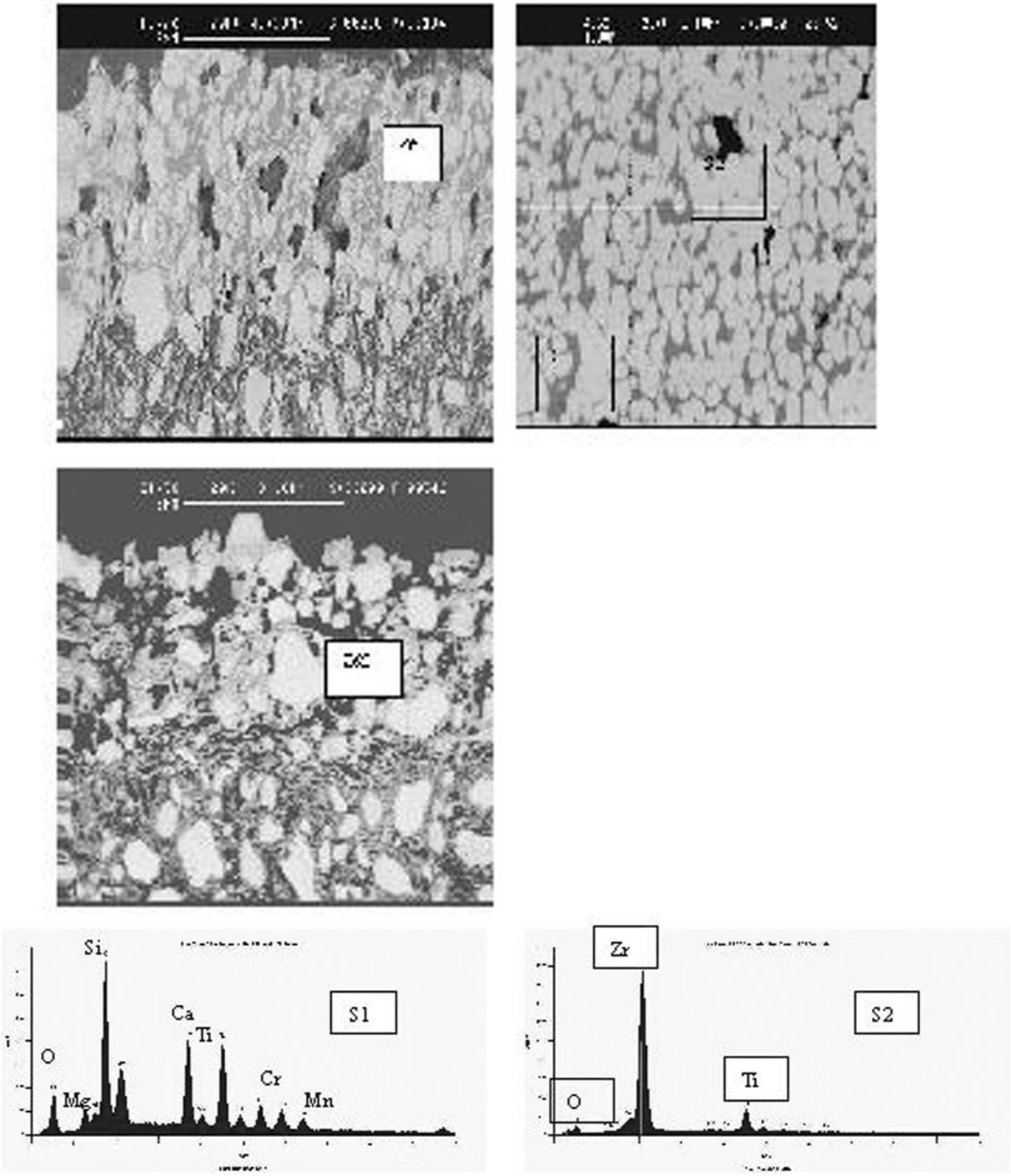

Figure 5. Penetration zones of Z6 and Z62. S1 shows a complex Si-Ti-Mg-Ca-Cr-O phase between particles of ZrO_2 with some Ti (S2)

hydration prior to testing. Figure 6 shows a cross section of the reacted samples of M1 (M2 showed a very similar interface zone with Ca also associated with the Ti-Si-Mg-O complex). Photomicrograph A shows a high magnification of the reaction zone for M1.

In the un-reacted state, M1 and M2 displayed MgO grains in an $MgO.SiO_2.CaO$ matrix, with the grain sizes being 500 and 100 μm respectively. M1 showed steel penetration of 3.5 mm and a complex reaction layer consisting of Ti rich Ti-Si-Ca-O and Ti-Mg-O. The surface of the layer is rough in comparison to the surfaces seen in Figures 2 to 5 and is potentially due to the hydration issue. Sample M2 exhibits similar phases to M1; however, there is a different distribution of CaO and MgO in the phases.

Lehmann *et al.*[12], in studying and modelling the reactions between a magnesia refractory and Al and Ti containing ultra low carbon steels, determined that spinels and a liquid phase rich in Al_2O_3 and TiO_2 form. In the current work, the rapid quenching of the samples, limited emersion time, and a high [Ti] to [Al] ratio, results in no spinel formation.

In the alumina based refractory L17, penetration depth was approximately 1.25 mm. In this case, the reaction zone consisted of Al-Si-Ca-O, Al rich Al-Si-Mg-Cr-Mn-O and $CaO-TiO_2$ entrapped particles. The Mn containing species was in the form of dendrites and was associated with entrapped steel particles.

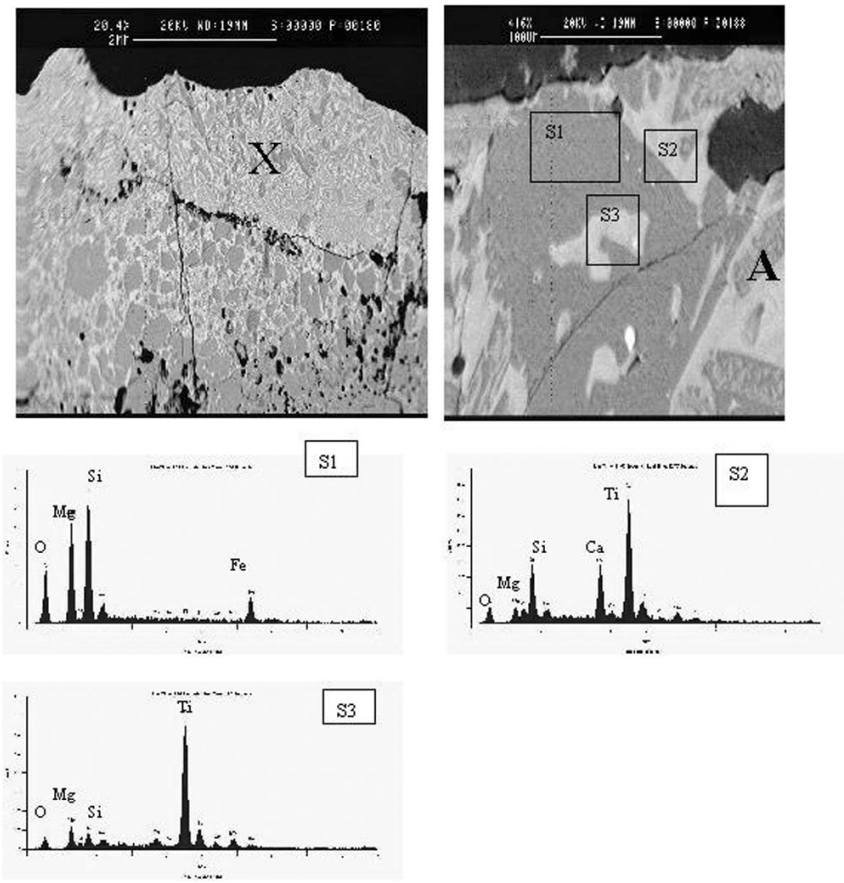

Figure 6. M1 sample with A being a higher magnification of X. S1 shows Mg-Si-O-(Ti); S2 shows Si-Ti-O-(Mg), and S3 Ti-Mg-O

Analysis of an equivalent chemistry $Al_2O_3.SiO_2$ castable product showed severe erosion in the plant environment. On investigation, it was determined that the size and distribution of the cement particles between the $Al_2O_3.SiO_2$ grains, as well as a higher proportion of SiO_2 particles, gave rise to increased penetration of the refractory. As highlighted above, the effect of SiO_2 is to change the activity of CaO, leading to modification of the networks.

A critical aspect of the dip test, which cannot duplicate the plant environment, is the lack of or limited flow of steel that occurs in an induction furnace. Therefore, the test indicates the potential reactions, which can occur without mechanical erosion. Due to the induction furnace being open to the atmosphere (high surface area to volume ratio), as well as the high test temperature, there was significant oxidation of the Ti from the steel. In the plant environment, the low surface area to volume ratio, lower operating temperatures and tundish slag cover, the oxidation of Ti is limited.

Tundish linings

In the continuing drive to improve the steel quality at Columbus, several developments have been made in the tundish area. Initially (1995) the tundish had a capacity for 15 T of steel and had an MgO based spray lining. With the improvements required for Ti stabilized steels[2], tundish furniture designs were tried[3] resulting in the use of an impact pad and baffle arrangement, Figure 1. In 2000, it was decided to trial an increased tundish volume, and the tundish was modified to 25 T capacity. Subsequent quality investigations as well as the impact on mould level control, particularly during ladle exchange periods, indicated that all tundishes should be changed to the 25 T size. By December 2002, all tundishes were converted.

Tundish slags have been developed at Columbus to aid in inclusion removal[2] and it was proposed that increasing the surface area available for inclusion removal should be investigated. This led to the utilization of an active tundish lining T2. T2 was applied to the standard working lining (T1) via gunning, with a resultant veneer of approximately 15 mm. Samples were taken from the steel/refractory interface after varying sequence lengths and for different grades. Utilizing EDS (effectively a semi-quantitative technique) on T2 yielded the results shown in Table VIII. Samples of T2 were also taken by the supplier and analysed by XRD. The samples were milled, mixed with a known proportion of SiO_2 and subsequently melted. The quenched buttons were then milled and prepared for XRD. The results are shown in Table IX as the measured value-original chemistry. The differences in results between the two techniques indicates that this form of analysis is not an accurate tool for a quantitative measurement of inclusion removal from the steel. The results do indicate that there is penetration of steel into the refractory to varying degrees.

Figure 7 shows a cross section of the reacted lining, with the photomicrographs covering approximately 7 mm. Photomicrograph A is from the surface to 1 mm, B is from 2 to 4 mm and C is from 5 to 7 mm. Figure 8 is a higher magnification of Figure 7 A and shows the associated EDS analyses of the phases present. B and C from Figure 7 show MgO particles in a $CaO-SiO_2-MgO-Al_2O_3$ matrix. Note the change in particle sizes from A to C. C also shows some porosity.

Table VIII
Results of semi-quantitative EDS analysis of T2

	Outer Layer		10 mm		15 mm	
	Av.	Std. Dev.	Av.	Std. Dev.	Av.	Std. Dev.
MgO	26.4	6.2	69.2	6.8	67.6	4.5
Al_2O_3	25.3	6.2	8.4	7.6	8.9	5.7
SiO_2	19.9	11.3	15.0	3.6	15.7	2.3
CaO	16.4	4.0	5.5	2.2	7.0	2.3
TiO_2	11.6	6.3	1.7	0.6	0.6	0.4
Total	99.6		99.8		99.8	

Table IX
XRD and EDS quantitative results for tundish lining T2. (Measured value-original specification)

Technique	Species	Face	10 mm	15 mm
XRD Button	Al_2O_3	8.5%	3%	1%
	SiO_2	12.0%	5%	5%
	TiO_2	14.1%	1%	0%
EDS	Al_2O_3	24.0%	7.1%	7.6%
	SiO_2	14.7%	11.8%	12.5%
	TiO_2	11.6%	0.6%	0.6%

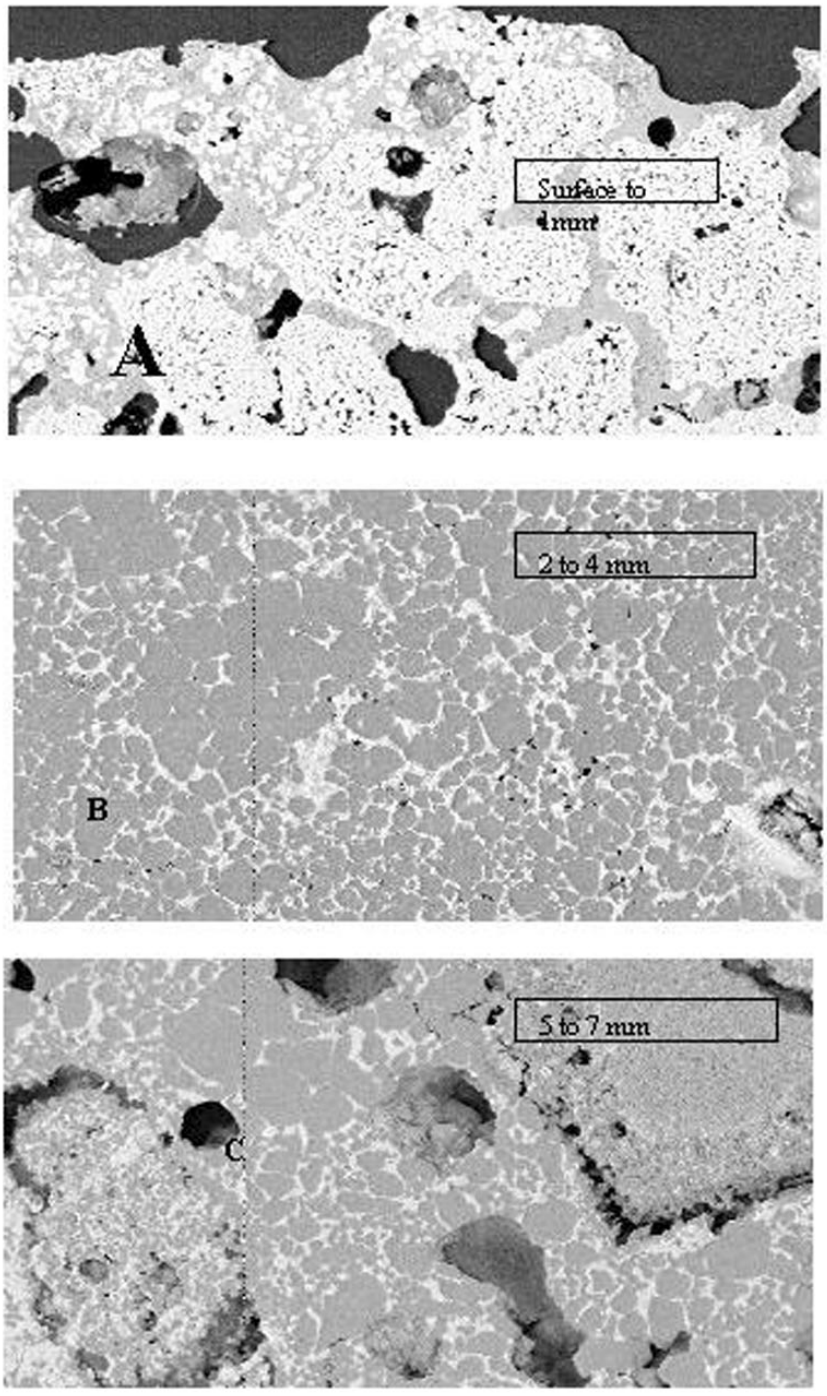

Figure 7. Tundish lining T2 after a 4 ladle sequence of 409. (A is shown in Figure 8 at a higher magnification). A is from the surface to 1 mm; B is from 2 to 4 mm and C is from 5 to 7 mm below the surface. Sections B and C show MgO particles in matrices of $CaO-SiO_2-MgO-Al_2O_3$. Section C also shows some porosity

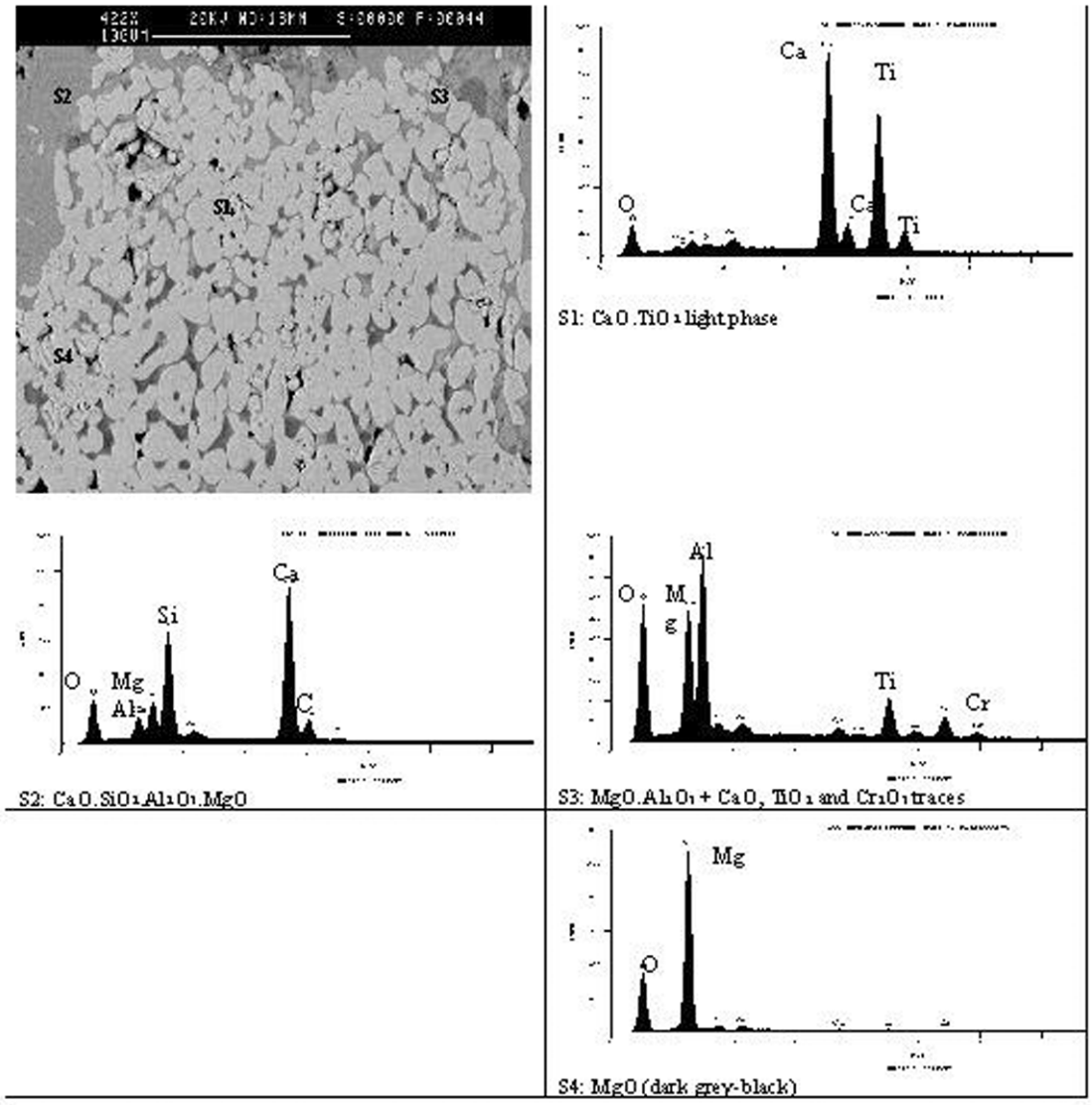

Figure 8. High magnification of Section A in Figure 7 S1 showsg $CaO.TiO_2$; S2 shows $CaO.SiO_2.Al_2O_3.MgO$,; S3 shows $MgO.Al_2O_3$ + $CaO.TiO_2$ and Cr_2O_3 traces; S4 shows MgO (dark/black particles)

The lack of carbon in the tundish linings reduces the opportunity for MgO reduction, thus limiting the formation of $MgO.Al_2O_3$ spinel (Al_2O_3 being a solubility product in 409). In Figure 8, S3 indicates that an $MgO.Al_2O_3$ spinel has formed in the reaction zone. For this spinel to form, there would be a requirement for a local Al_2O_3 content of at least 20% in a liquid slag. The tundish slag utilized has a bulk Al_2O_3 content of 16%; however with inclusion pick-up and erosion of refractories the Al_2O_3 content changes[2]. The size of the spinel indicates that it formed over a period of time, and supports the premise presented by Riaz *et al.*[4] and Hassall *et al.*[5], whereby a slag glaze is left on the lining with each draining and filling step. The CaO content of T2 allows the formation of $CaO.TiO_2$ and $CaO.SiO_2$ as evidenced in Figure 8. Nunnington and Sutcliffe[2] showed that the tundish slag has a high affinity for SiO_2, Al_2O_3 and TiO_2 with perovskite forming at approximately 15 to 18% TiO_2. Investigations of the downstream quality indicated an increase in the number of metallurgical defects on the heats produced in the trial tundishes. The defects were analysed to be predominantly perovskite and calcium silicate. In contrast, T1 and T3 show very little Ti-Ca-O or Si-Ca-O phases.

In December 2002, a further step in the development of tundish practices for clean steel production, as well as to allow an increased sequence length, was the implementation of 'dry-vibe' tundish linings. These linings are a high MgO product with a binder, which has a curing cycle of 2 to 3 hours; a similar practice has been presented by Grip *et al.*[18]. The traditional spray tundish can give rise to hydrogen pick-up, tundish wall collapses due to incorrect water additions, as well as causing damage to the back lining during de-skulling.

The tundishes are pre-heated to 1100°C prior to being filled with steel, and samples of T3 were taken on and below the slag line from a 4-ladle sequence of 409. Figure 9 shows the slag/refractory reaction zone. No Ti based inclusions or phases were observed in the slag/refractory interaction zone.

Figure 10 shows a photomicrograph of the steel/refractory reaction zone. T3 shows the least steel penetration of all of the tundish linings tested, at 0.15 mm. Distinct $CaO.TiO_2$ (perovskite) and Cr-Al-O particles are seen in a CaO rich Ca-O-Si matrix in the reaction zone. Based on the EDS analysis of the Ca-O-Si phase, it is proposed that the phase is di-calcium silicate. The melting

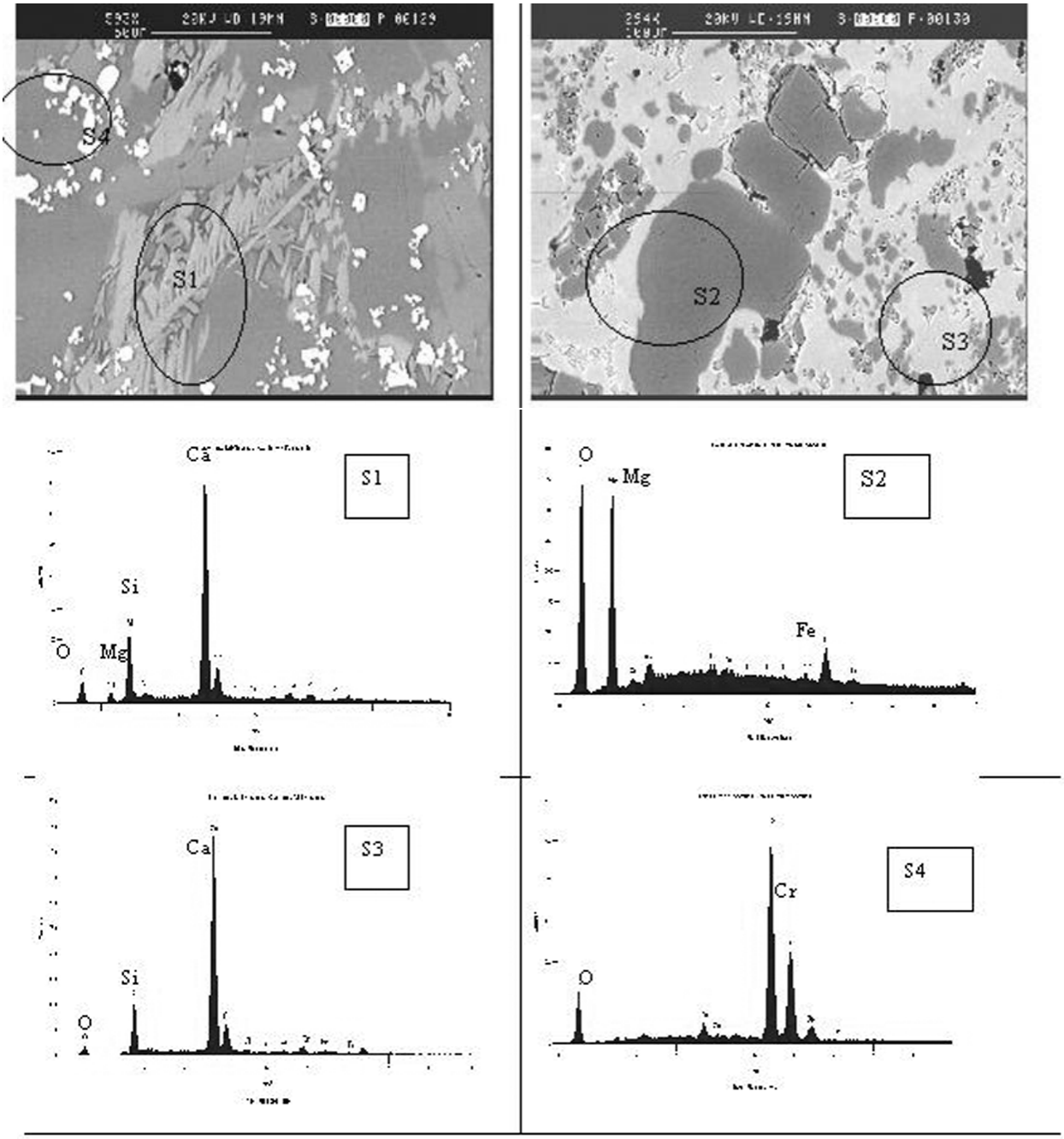

Figure 9. T3 slag/refractory interface showing dendritic type structure of Ca-Si-Mg-O (S1), MgO (S2), 2CaO.SiO_2 (S3) and Cr-O metallic blebs (S4)

point of this phase is above the 1550°C tundish steel temperature, and is therefore presumed to be stable. EDS analysis of T3 showed that Cr, Mn and Ti oxides were all below 1% and thus to determine the change in refractory chemistry with depth, the system was normalized around CaO, MgO and SiO_2 (Table X). At the slag/refractory reaction site, there is a reduction in the MgO content of the material, due to the tundish slag not being saturated in MgO, to a depth of 6 mm. At the steel/refractory reaction site, the SiO_2 and CaO content are stable throughout the lining. Analysis of downstream quality of steel produced in the 'dry-vibe' tundishes indicated an improvement in slab quality. To date the tundish has allowed casting for 14 hours without any damage to the back-lining and minimal erosion.

Conclusions

- The simple dip tests performed in this work have shown penetration mechanisms equivalent to plant samples. This allows off-line analysis of new products without interfering with plant operation. The effect of erosion from steel flow can, however, not be modelled with the current dip test
- The size distribution of particles within the refractory play an important role in the extent of steel penetration. The distribution pattern within the refractory influences the uniformity of the penetration front
- Various complex network layers formed on the base refractory. The potential reactions have been outlined and referenced with published results. The competing reactions of decarburization and reduction of oxides in

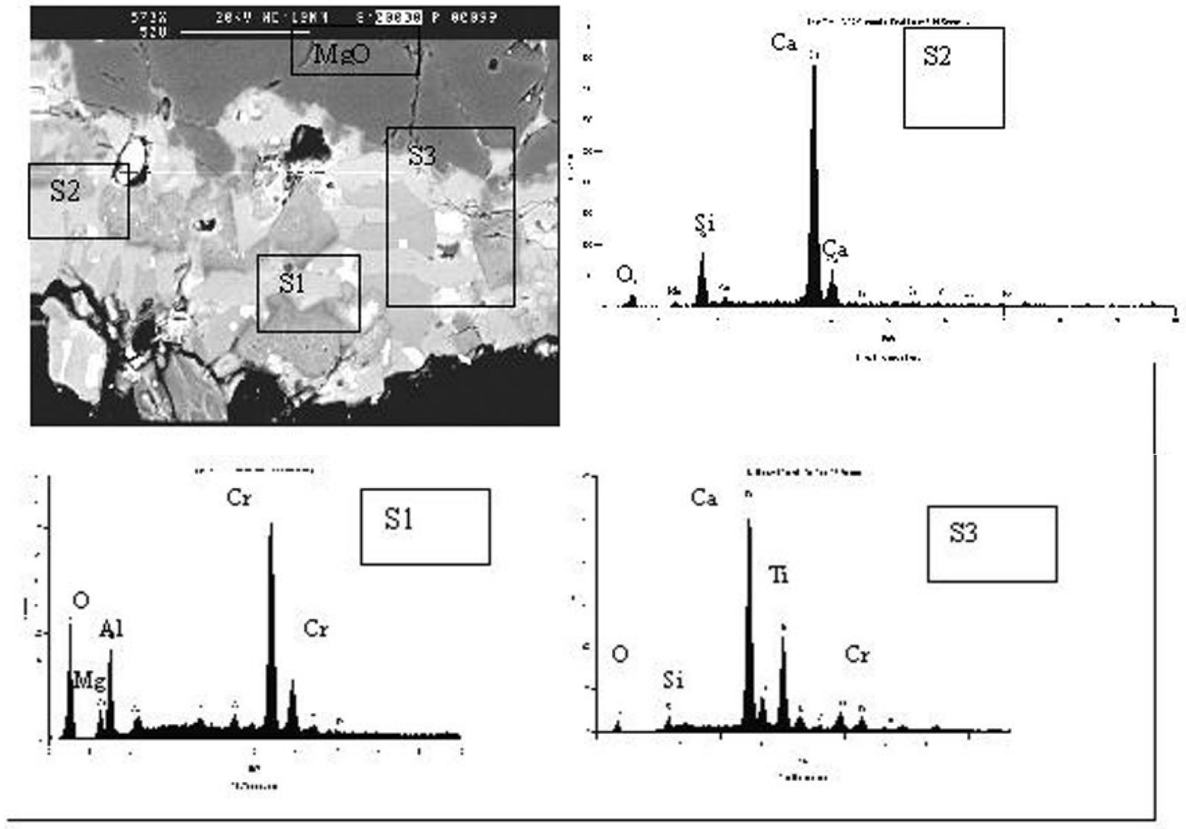

Figure 10. T3 steel/refractory interface showing Cr-Al-Mg-O (S1), 2CaO.SiO2 (S2), $CaO.TiO_2$ (S3) with the metallic blebs being Ti-Cr

Table X
EDS analyses of the interaction between steel and T3 and slag and T3. Position relates to depth below the surface

Steel/Refractory				Slag/Refractory		
Position mm	MgO	SiO_2	CaO	MgO	SiO_2	CaO
1	66	10	24	35	29	34
2	63	12	25	47	23	28
3	61	13	26	57	25	32
4	66	13	21	49	24	28
5	62	12	26	47	23	27
6	59	13	28	44	22	30
7	59	13	28	60	20	24
8	62	13	25	58	17	21
9	60	12	28	62	16	23
10	56	12	32	57	20	21
11	65	18	17	62	20	24
12	65	16	19	56	19	25
13				55	19	24
14				55	18	25
15				59	19	22

the refractory, and the reduction of oxides in the refractory by elements in the steel, results in this complex network formation

- The correct choice of ZrO_2 grain size and distribution and the level of SiO_2 in the mix, radically affects the penetration behaviour in steel. This has consequences for the development of protection bands for SENs
- The utilization of MgO based castables at present is not viable due to the influence of hydration. $Al_2O_3.SiO_2$ castables are preferable with the correct grain sizes and phase assemblage
- The presence of CaO in the tundish linings resulted in significant penetration and erosion and affected the final product quality negatively
- The 'dry-vibe' tundish lining shows minimal penetration and limited erosion.

Acknowledgements

The assistance of Columbus laboratory personnel, particularly A. Freire, P. Rootman, G. du Preez and D. Pieterse in the SEN analysis is gratefully appreciated. The author wishes to thank the Columbus management for permission to publish this work. The supply of materials by various suppliers, as well as detailed discussions, was most beneficial.

References

1. SUTCLIFFE, N. and NUNNINGTON, R.C. Slag control for sulphur reduction in a stainless steel making process. *6th International Conference on Molten Slags, Fluxes and Salts*, Stockholm and Helsinki. June 2000.
2. NUNNINGTON, R.C. and SUTCLIFFE, N. The steelmaking and casting of Ti stabilized stainless steels. *59th Electric Furnace Conference*, Phoenix, November 2001.
3. ACKERMAN, M.J. and ORBAN, W.G. A perspective of practical issues relating to tundish development. *85th Steelmaking conference proceedings*, 2002. pp. 409–418.

4. RIAZ, S., CEDERLUND-LOSENBORG, A., MILLS, K.C., and BAIN, K. Characterisation and entrapment of ladle glazes in the molten steel. *6th International Conference on Molten Slags, Fluxes and Salts*, Stockholm and Helsinki. June 2000.

5. HASSALL, G.J., BAIN, K.G., JONES, N., and WARMAN, M.O. Modelling of ladle glaze interactions. *Ironmaking and Steelmaking*, vol. 29, no. 5. 2002. pp. 383–389.

6. MATTILA, J.R., VATANEN, J.P., and HARKKI, J.J. Chemical wearing mechanism of refractory materials in a steel ladle slag line. *6th International Conference on Molten Slags, Fluxes and Salts*, Stockholm and Helsinki. June 2000.

7. MUKAI, K., TAO, Z., GOTO, K., LI, Z., and TAKASHIMA, T. *In situ* Observation of Slag Penetration into MgO refractory. *6th International Conference on Molten Slags, Fluxes and Salts*, Stockholm and Helsinki. June 2000.

8. BRABIE, V. Mechanism of reaction between refractory materials and aluminium deoxidized molten steel. *ISIJ International*, vol. 36, supplement, 1996. pp. S109–S112.

9. JONES, P.T., BLANPAIN, B., WOLLANTS, P., DING, R., and HALLEMANS, B. Degradation mechanisms of magnesia-chromite refractories in vacuum-oxygen decarburisation ladles during production of stainless steels. *Ironmaking and Steelmaking*, vol. 27, no. 3, 2000. pp. 228–237.

10. CIRILLI, F., DI DONATO, A., DUPEL, P., and GUILLO, P. Fundamental mechanisms in chemical interaction between C-bonded refractories and steel. (Poster). *6th International Conference on Molten Slags, Fluxes and Salts*, Stockholm and Helsinki. June 2000.

11. KWON, O.D., YIM, C.H., and RHEE, C.H. Comparison of network layer formation behaviour between Al_2O_3-SiO_2-C continuous casting nozzle and molten steels with the change of Al and Ti content. *7th Biennial Worldwide Congress*, UNITECR'01, Cancun, Mexico. November 2001.

12. LEHMANN, J., BOHER, M., SOULARD, H., and GATELLIER, C. Metal/Refractory interactions: A thermodynamic approach. *7th Biennial Worldwide Congress*, *UNITECR'01*, Cancun, Mexico. November 2001.

13. MATSUSHITA, T., OHUCHI, T., MUKAI, K., SASAKA, I., and YOSHITOMI, J. Direct observation of molten steel penetration into porous refractory. Journal of the *Technical Association of Refractories*, Japan, 23 [1]. 2003. pp. 15–19.

14. MOULDEN, G.T. and SABOL, R. Development of doloma tundish nozzles to reduce alumina clogging. *I&SM*, June 2000, pp. 35–38.

15. VERMEULEN, Y., COLETTI, B., BLANPAIN, B., WOLLANTS, P., and VLEUGELS, J. Material evaluation to prevent nozzle clogging during continuous casting of Al killed steels. *ISIJ International*, vol. 42, no. 11, 2002, pp. 1234–1240.

16. HAK DONG, L. and SIK, S. Chemical relationship between components of mould powder and partially stabilised Zirconia on the corrosion of submerged entry nozzle. *3rd International Symposium on Refractories*, Beijing, China, November 1998. pp. 103–109.

17. UCHIDA, K. Influence of Zirconia grain size on corrosion resistance of Zirconia graphite material. *Journal of the Technical Association of Refractories,* Japan, 22[3] 2002, pp. 214–218.

18. GRIP, C.E., EKBERG, S., and LINDBLOM, B. Reactions between slag and a dry-hardened tundish lining. *6th International Conference on Molten Slags, Fluxes and Salts*, Stockholm and Helsinki. June 2000